ADVANCED MATERIALS
www.advmat.de

An Overstretch Strategy to Double the Designed Elastic Stretchability of Stretchable Electronics

*Juyao Li, Xiaolei Wu, and Yewang Su**

Achieving or enhancing the elastic stretchability of inorganic stretchable electronics is critically significant. However, only two types of fundamental strategies—using the prestrained elastic substrate and designing the geometric layouts—are exploited thus far. This study proposes a third strategy, an overstretch strategy, applied beyond the designed elastic range of stretchable structures after transfer printing and bonding to a soft substrate. The theoretical, numerical, and experimental results collectively prove that the overstretch strategy can double the designed elastic stretchability of fabricated stretchable electronics and is valid for various geometrical interconnects with both thick and thin cross-sections. The underlying mechanism is that the elastic range of the critical part of the stretchable structure is doubled, owing to the evolution of the elastoplastic constitutive relation during overstretching. The overstretch strategy can be easily executed and combined with the other two strategies to enhance elastic stretchability, which has profound implications for the design, fabrication, and applications of inorganic stretchable electronics.

1. Introduction

Stretchable electronics have been extensively developed in the last decade for diverse applications ranging from health monitoring,[1–6] medical treatment,[7–9] and intelligent industries[10,11] to aerospace equipment[12] with stretchable or curvilinear characteristics. The key technological innovation in inorganic stretchable electronics (this study is limited to inorganic stretchable electronics) is the achievement of elastic stretchability through the designed mechanical structures, enabling conformal wrapping on arbitrarily complicated target surfaces, maintaining the electronic functions unchanged. For instance, the "island–bridge" mesh structure, in which the functional components reside at the "islands" and the interconnects form the "bridges," is the most popular one. The "islands" undergo negligible deformation during the stretch of the structure, and the "bridges" provide both elastic stretchability and electronic conductivity. Strategies for achieving elastic stretchability of stretchable electronics are critically essential and have attracted significant research attention.

Although several previous studies have focused on the design of stretchable structures, as shown in **Figure 1**,[13–21] only two fundamental strategies have been exploited to achieve or enhance elastic stretchability. These strategies are described as follows. 1) By using the prestrained elastic substrate; a waved ribbon is a typical example.[19] A pre-strain is applied to the elastic substrate before the straight planar ribbon is transfer-printed and bonded. The release of the prestrain yields compression and out-of-plane buckling of the transfer-printed ribbon, forming a waved shape with stretchable characteristics. Besides, more complex stretchable 3D mesostructures are fabricated by 2D precursors bonded to prestrained elastic substrates.[22,23] 2) By designing geometric layouts; versatile stretchable structure layouts involving curved interconnects have been designed; these include horseshoe,[24–26] serpentine,[21,27] fractal,[28–30] non-buckling,[16,31] helical structures,[32] and kirigami-inspired structures[33] which exhibit different features in terms of elastic stretchability and application scenarios. Sometimes, the two types of strategies are combined to enhance the stretchability of mechanical structures. For instance, a prestrained elastic substrate significantly increases the stretchability of serpentine structures.[13]

As the third type of strategy (**Figure 2**), this study proposes overstretching beyond the designed elastic range of stretchable structures, applied after transfer printing and bonding to the soft substrate. The overstretch strategy can double the designed elastic stretchability, which is critical for the performance of stretchable electronics. The theoretical, numerical, and experimental results collectively prove that the overstretch strategy is valid for various geometrical interconnects with both thick and thin cross-sections. The underlying mechanism is revealed owing to the evolution of the elastoplastic constitutive relation of the critical part of the stretchable structures during overstretching. The overstretch strategy can be easily executed and combined with the other two strategies to enhance elastic stretchability, which has

J. Li, X. Wu, Y. Su
State Key Laboratory of Nonlinear Mechanics
Institute of Mechanics
Chinese Academy of Sciences
Beijing 100190, China
E-mail: yewangsu@imech.ac.cn
J. Li, X. Wu, Y. Su
School of Engineering Science
University of Chinese Academy of Sciences
Beijing 100049, China

The ORCID identification number(s) for the author(s) of this article can be found under https://doi.org/10.1002/adma.202300340

DOI: 10.1002/adma.202300340

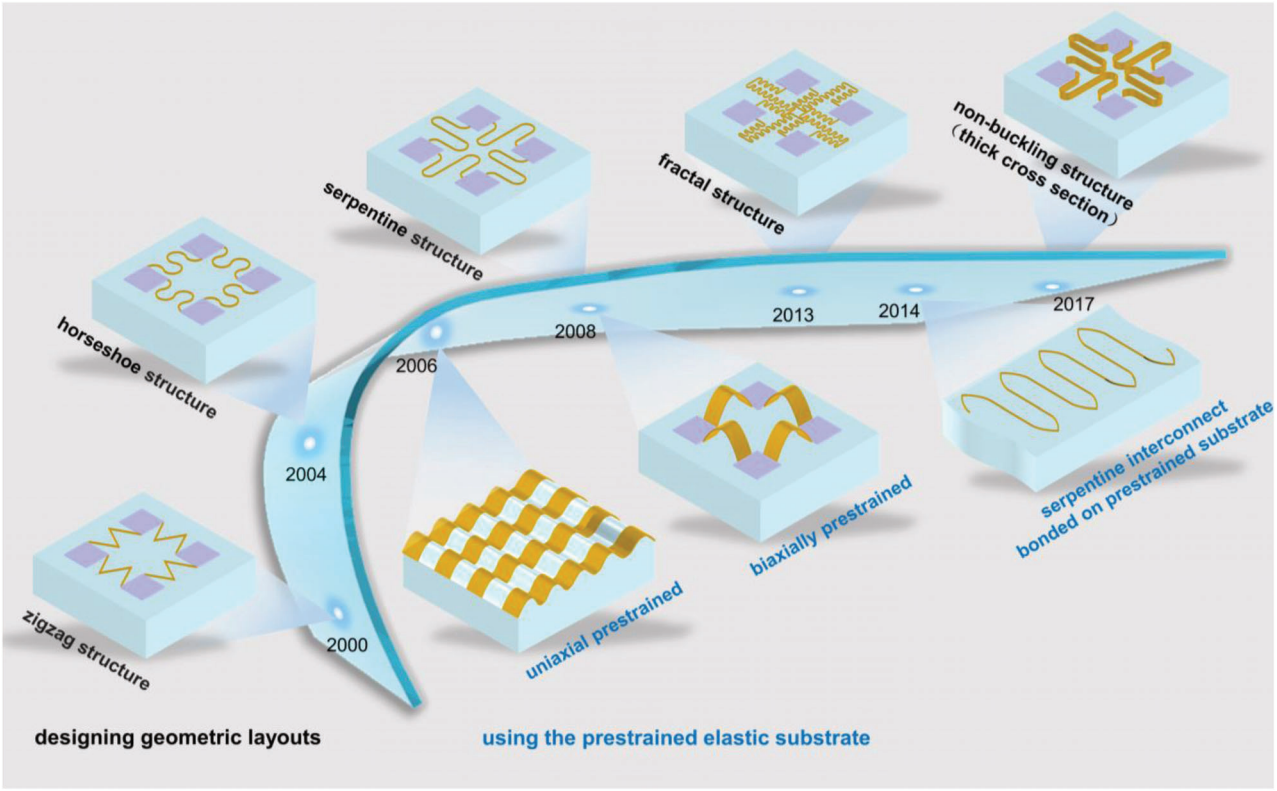

Figure 1. Evolution of stretchable structures over the past decades.

profound implications for the design, fabrication, and applications of stretchable electronics.

2. Results and Discussion

2.1. Demonstration of the Overstretch Strategy

For example, Figure 2 shows a schematic of the overstretch strategy to enhance the stretchability via metallic thick serpentine interconnects (MTSI) with $R = 0.25$ mm for the radius of the semicircle, $L = 3$ mm for the length of the straight portion, and $w \times t_{inter} = 50\ \mu m \times 100\ \mu m$ for the cross-section, bonded on a soft substrate with a thickness of $t_{sub} = 1$ mm. The column on the left (Column 1) shows the step-by-step operations of the overstretch strategy, and Columns 2 and 3 present the contours of the finite element analysis (FEA) for the maximum principal strain and equivalent plastic strain of the MTSI, respectively. However, for simplicity, ideal elastoplasticity (**Figure 3**a) and the hyperelasticity of the Mooney–Rivlin model are adopted for the mechanical constitutive relationships of the MTSI and the soft substrate, respectively.

$$\sigma = \begin{cases} E_{metal}\epsilon, & |\epsilon| \le \frac{\sigma_s}{E_{metal}} \\ \sigma_s, & |\epsilon| > \frac{\sigma_s}{E_{metal}} \end{cases} \quad (1)$$

In Equation (1), σ is the stress, ϵ is the strain, E_{metal} is Young's modulus, and σ_s is the yield stress. In this example, $E_{metal} = 124$ GPa and $\sigma_s = 350$ MPa for copper; $C_{10} = 0.008054$ MPa, $C_{01} = 0.002013$ MPa, and $D_1 = 2\ \text{MPa}^{-1}$ in the Mooney–Rivlin model are used for the soft substrate.

In regime ①, the MTSI is transfer-printed and bonded on the soft substrate. The entire structure is stress/strain-free. The maximum stress reaches the yield stress σ_s at the cross-section of the semicircle vertex in regime ②, whereas the first applied strain $\epsilon_{first\text{-}applied}$ reaches the designed elastic stretchability $\epsilon_{designed\text{-}elastic}$ (58.5%). During stretching from regime ① to ②, the deformation of the MTSI involves only pure elasticity without any plasticity. This is the conventional definition of elastic stretchability for stretchable electronics. The addition of the first applied strain yields plastic deformation, as shown in regime ③. The cross-section of the semicircle vertex of the MTSI represents the yield behavior and the equivalent plastic strain increases. Even if a large local plasticity exists in the section, the remaining portion can withstand the external load. Thus, the MTSI can withstand 140% of the applied strain without damage. After the release of the overstrain ϵ_{over} (140%, a value more than twice the designed elastic stretchability), which is the maximum of the first applied strain, the soft substrate almost restores to its original regime, and the MTSI is returned to its original state, as depicted in regime ④. In this process, elastic unloading, elastic reverse loading, and plastic reverse loading occur successively at the cross-section of the semicircle vertex of the MTSI, where the stress distribution becomes rather complicated. The maximum principal strain decreases, whereas the equivalent plastic strain increases. After the complete execution of the overstretch strategy from ① to ④, the MTSI bonded to the soft substrate can be reloaded. In the process from regime ④ to ⑤, the second applied

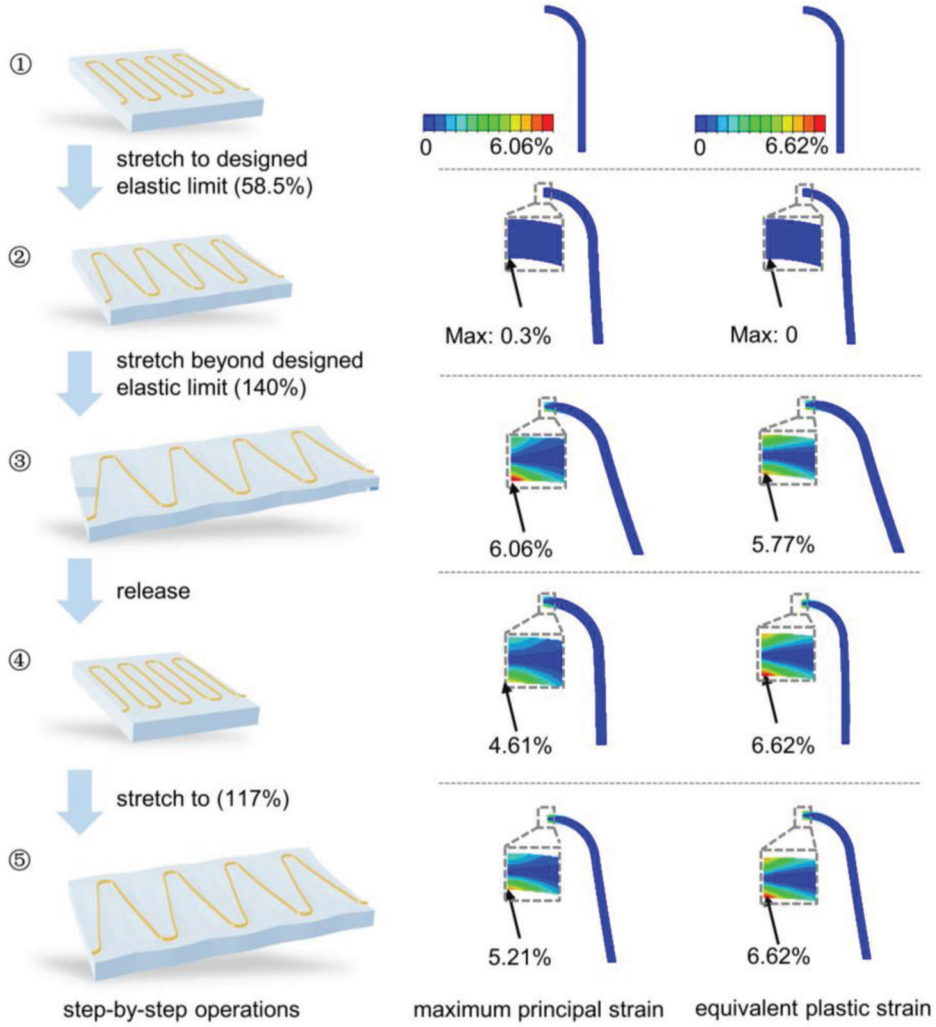

Figure 2. Operation of the overstretch strategy. The column on the left (Column 1) shows the step-by-step operation of the overstretch strategy: ①,② stretching to the designed elastic limit (58.5%), ②,③ stretching beyond the designed elastic limit (140%), ③,④ releasing the applied strain, ④,⑤ stretching to enhanced elastic limit (117%). Columns 2 and 3 provide the contours of the FEA for the maximum principal strain and equivalent plastic strain of the MTSI corresponding to each step in Column 1, respectively.

strain is 117%, which is as large as twice the designed elastic stretchability (58.5%); however, it does not yield any increment of the equivalent plastic strain. The increment in the maximum principal strain (0.6%) at the semicircle vertex, which is twice that from regime ① to regime ② (0.3%), is purely elastic. The maximum second applied strain, which does not result in any plasticity, is defined as enhanced elastic stretchability $\epsilon_{\text{enhanced-elastic}}$. In short, after the operation from regime ① to ④, that is, the execution of the overstretch strategy, the enhanced elastic stretchability $\epsilon_{\text{enhanced-elastic}}$ can be twice that of the designed elastic stretchability $\epsilon_{\text{designed-elastic}}$.

2.2. Mechanical Model, Mechanism Analysis, and Experimental Verification via the Freestanding MTSI

To understand the underlying mechanism quantitatively, a freestanding MTSI without a soft substrate is adopted for analysis and modeled as slender beams with in-plane deformation, as shown in Figure 3b. Based on periodicity, the operation process is demonstrated for one period, as shown in Figure 3c. Mechanical analysis is applied to a quarter of a period, as depicted in the subgraph of Figure 3b, owing to its symmetricity. Based on the linear elastic theory of beams, the designed elastic stretchability from regime ① to ② can be obtained as (See Supporting Information for further details, Supporting Information Appendix)

$$\epsilon_{\text{designed-elastic}} = \frac{\sigma_s}{EwR(R+L)}\left[\frac{\pi R}{2}\left(R^2+2L^2\right)+\frac{2L}{3}\left(6R^2+L^2\right)\right] \tag{2}$$

In the stretch process from regime ① to ②, the deformation of the MTSI involves only pure elasticity without any plasticity (Figure 3c). The stress is linearly distributed along the cross-section of the MTSI. The elastic stretchability is not enhanced

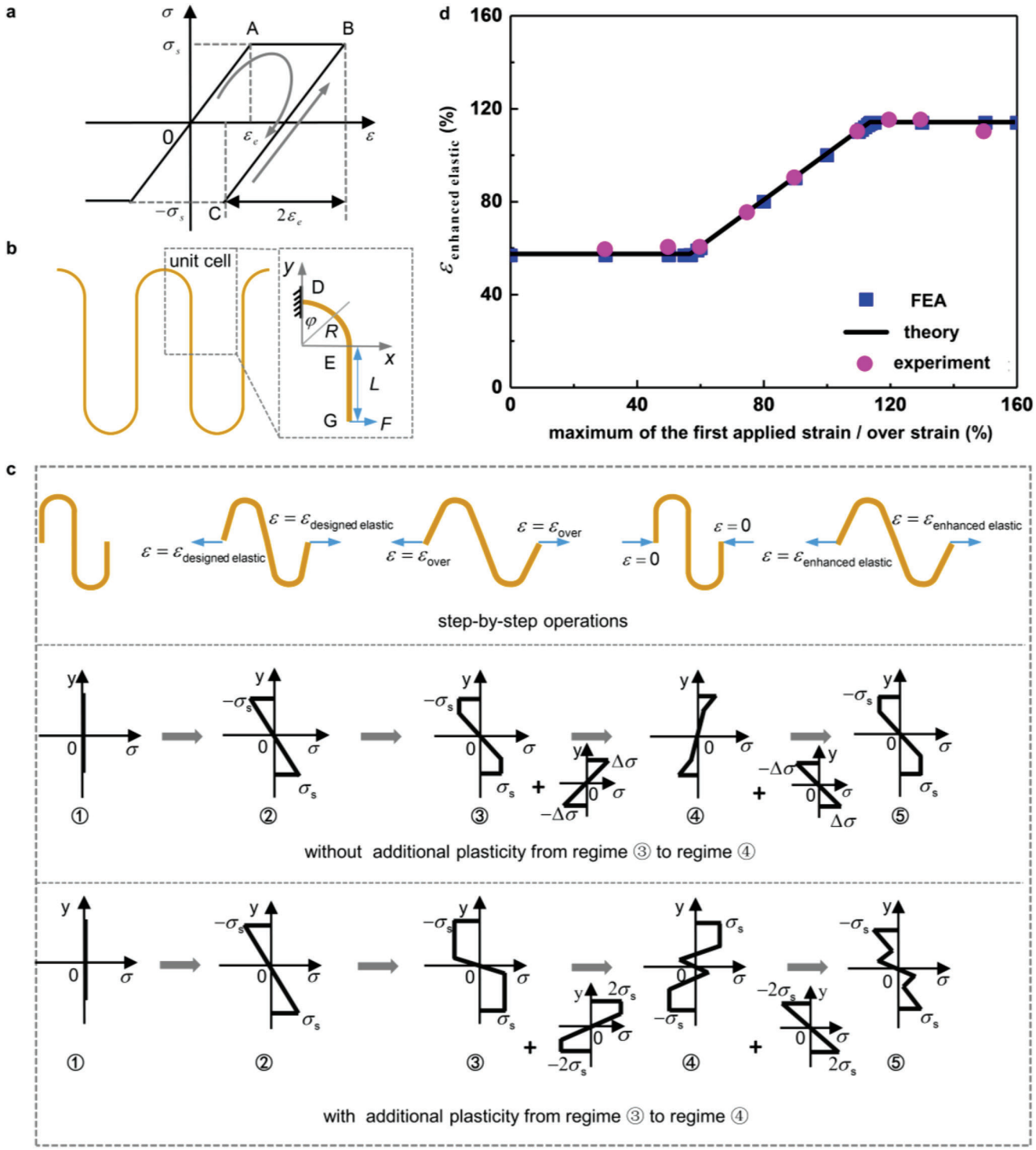

Figure 3. Mechanical analysis of the overstretch strategy via the freestanding MTSI. a) Mechanical constitutive relationship of the MTSI: ideal elasto-plasticity. b) Schematic and mechanical model of the freestanding MTSI. c) First row: step-by-step overstretch strategy operation with freestanding MTSI (one period). Second row: stress distribution in the cross-section of the semicircle vertex in each process if no additional plasticity occurs from regime ③ to ④. Third row: stress distribution in the semicircle vertex cross-section in each process if additional plasticity occurs from regime ③ to ④. d) Enhanced elastic stretchability of the freestanding MTSI as a function of the maximum of the first applied strain/overstrain, including the results of the experiments, FEA, and theory.

if an overstretch beyond the designed elastic stretchability is not applied, as shown in the left horizontal line of Figure 3d. Here, the same geometric and material parameters are used with the MTSI shown in Figure 2, but without the soft substrate.

The addition of the first applied strain yields plastic deformation, as shown in regime ③ ($\epsilon_{\text{first-applied}} = \epsilon_{\text{over}}$), aiming to enhance the elastic stretchability. It is a critical question whether the reverse displacement unloading from regime ③ to regime ④ ($\epsilon_{\text{first-applied}} = 0$) results in additional plasticity. It can be analyzed based on the mechanical behavior of the stress of the semicircle vertex during reverse displacement unloading (Figure 3c). The change in the maximum stress can be as large as $2\sigma_s$ if only elastic unloading and elastic reverse loading occur, without any plastic reverse loading. Therefore, the replacement of σ_s by $2\sigma_s$ in Equation (2) determines the range of the overstretch ϵ_{over}, that is $\epsilon_{\text{over}} \leq 2\epsilon_{\text{designed-elastic}}$. Vice versa, the second applied strain $\epsilon_{\text{second-applied}}$ up to ϵ_{over} subsequently does not result in any plasticity from regime ④ to ⑤. Therefore, the enhanced elastic stretchability can be obtained as

$$\epsilon_{\text{enhanced-elastic}} = \epsilon_{\text{over}} \text{ for } \epsilon_{\text{designed-elastic}} < \epsilon_{\text{over}} \leq 2\epsilon_{\text{designed-elastic}} \quad (3)$$

as shown in the middle diagonal line of Figure 3d.

In the case of $\epsilon_{\text{over}} > 2\epsilon_{\text{designed-elastic}}$, the reverse process from regime ③ to regime ④ results in additional plasticity, as depicted in the subgraphs in the bottom column of Figure 3c, which is different from the above case. However, the stress analysis of the semicircle vertex shows that the change in the maximum stress does not exceed $2\sigma_s$ for the second applied strain. Therefore, the enhanced elastic stretchability does not exceed twice the designed elastic stretchability, that is,

$$\epsilon_{\text{enhanced-elastic}} = 2\epsilon_{\text{designed-elastic}}, \text{ for } \epsilon_{\text{over}} > 2\epsilon_{\text{designed-elastic}} \quad (4)$$

as indicated by the right horizontal line in Figure 3d. Based on the above results, an optimal value exists for the first applied strain, that is $\epsilon_{\text{over-optimal}} = 2\epsilon_{\text{designed-elastic}}$. At this point, the overstretch strategy can double the elastic stretchability and does not yield unnecessary plasticity.

The underlying mechanism can be further examined by focusing on the evolution of the constitutive relationship of the semicircle vertex, as shown in Figure 3a. Here, only the part with a positive strain is discussed without losing generality. In the stretching process from regime ① to regime ②, the status of the constitutive relationship involves the range of OA, which corresponds to the designed elastic stretchability $\epsilon_{\text{designed-elastic}}$. During the overstretch process from regime ② to ③, the status of the constitutive relationship is extended to OAB, consisting of both elastic and plastic behaviors. The unloading process from regime ③ to ④ is rather complicated, involving the entire OABC. However, the reloading process from regime ④ to ⑤ involves only OA and BC, which are both in the elastic range. The essential change during overstretching is that the status of the constitutive relation moves from OA to BC for the critical part of the MTSI. Therefore, the elastic range of the constitutive relationship and designed elastic stretchability are both doubled.

Experiments were conducted to verify these theoretical conclusions. As shown in **Figure 4**a, an MTSI consisting of four periods is fabricated and tested. The ideal elastoplastic model with Young's modulus $E_{\text{metal}l} = 124\text{GPa}$ and yield stress $\sigma_s = 350\text{MPa}$ can sufficiently describe the constitutive relationship of the metal (copper) (Figure 4b). The above operation process, including the first applied stretch, reverse unloading, and second applied stretch, is applied to the MTSIs with different maximum values of the first applied strain/overstrain for each MTSI. The curves of force versus applied strain plotted in Figure 4c–k from experimental testing consistently verify the theoretical prediction. For the first applied strain below 60%, no plasticity is observed during the operation of the first applied stretch, reverse displacement unloading, and second applied stretch. The elastic stretchability is not enhanced, and the designed value is maintained (60%) (See Supporting Information Appendix for further details,). For the first applied strain $60\% < \epsilon_{\text{over}} \leq 120\%$, the curve of the second applied stretch overlaps with that of the reverse displacement unloading. This implies that the MTSI undergoes elastic deformation without any plasticity during the overlapping of the curves. The enhanced elastic stretchability satisfies Equation (3) (see Supporting Information for further details; Supporting Information Appendix). For the first applied strain $\epsilon_{\text{over}} > 120\%$, the curve of the second applied stretch is clearly distinguished from that of the reverse displacement unloading. This indicates that the reverse displacement unloading results in additional plasticity. However, determining the elastic range of the second applied stretch (the enhanced elastic stretchability $\epsilon_{\text{enhanced-elastic}}$) is still essential. Comparing the experimental testing and theoretical and numerical analyses reveals that the enhanced elastic stretchability does not exceed 120%, although overstretching is applied to values as large as 130% and 150% (See Supporting Information Appendix for further details,). The experimental results obtained from Figure 4c–k and the FEA results plotted in Figure 3d are consistent with the theoretical prediction, thus verifying the feasibility and effectiveness of the overstretch strategy.

Additionally, plastic hardening (isotropic or kinematic) must be considered for certain materials. Considering the linear hardening constitutive relationship with the hardening modulus $E_{\text{hardening}} = 12.4$ GPa as an example, the enhanced elastic stretchability can be more than twice the designed elastic stretchability for isotropic hardening because the stress variation of the semicircle vertex can exceed $2\sigma_s$; however, it can only double the designed elastic stretchability for kinematic hardening (Figure S3, Supporting Information Appendix) because the stress variation of the semicircle vertex does not exceed $2\sigma_s$. It is also worth noting that a small deformation is assumed so that a simple analytic solution can be obtained to quantitatively present the mechanism without losing the essence of the overstretch strategy. The deformation of the MTSI mainly includes bending of the semicircle and rotation of the straight portion. As the straight portion is relatively long, the small rotation yielded by the bending of the semicircle can induce a large displacement of the straight portion, that is, an evident deformation of the MTSI. Thus, the mechanical theory with a small deformation assumption is applicable within a reasonable range. The FEAs with finite and small deformation assumptions are performed to verify the analytical model with a small deformation assumption. The results shown in Figure S4 (Supporting Information) indicate that the effect of geometric nonlinearity is very small for $\epsilon_{\text{over}} < 2\epsilon_{\text{designed-elastic}}$. For larger ϵ_{over}, such as 200%, the error is acceptable.

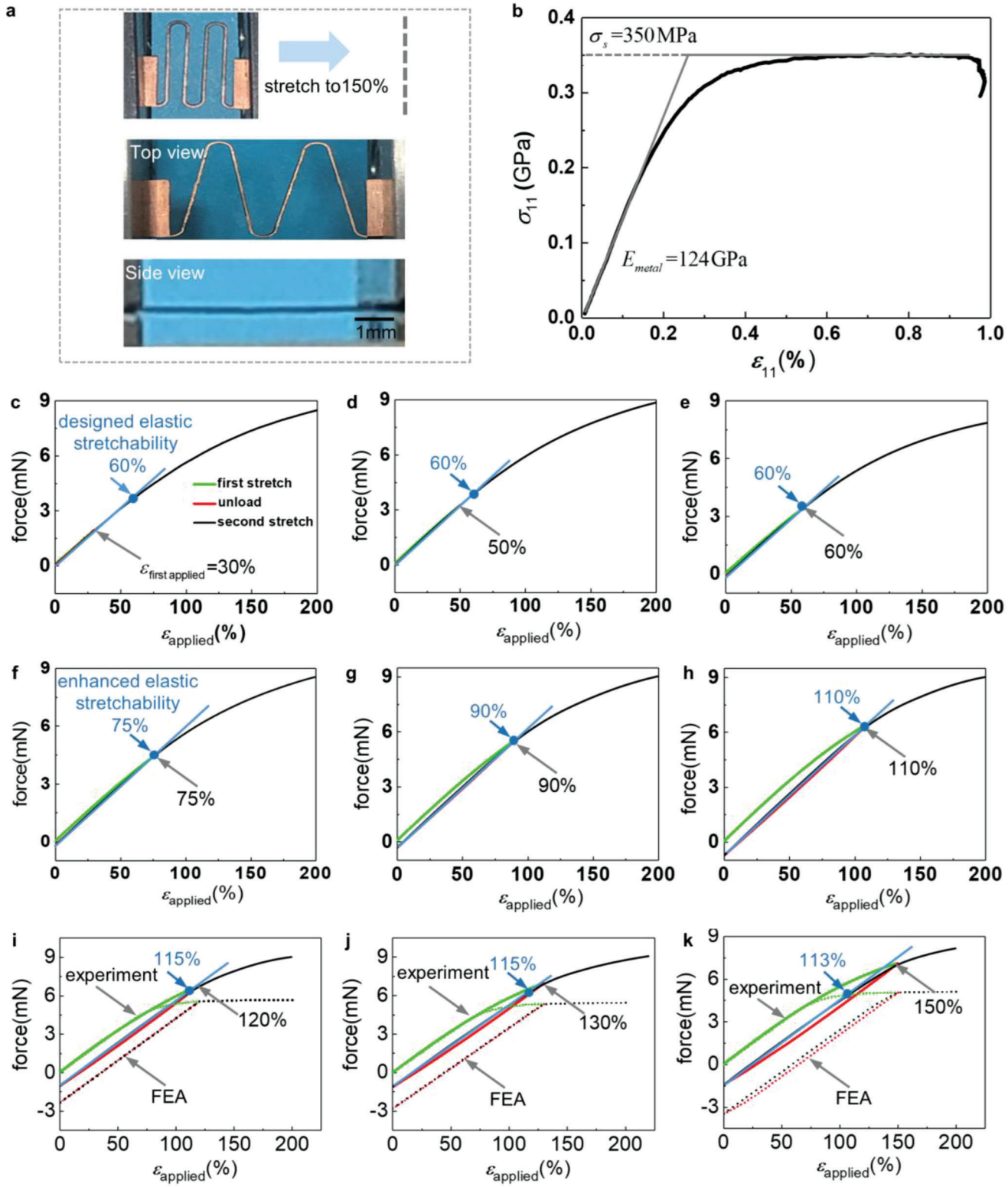

Figure 4. Experimental verification of the overstretch strategy via the freestanding MTSI (thickness t_{inter} = 100 µm). a) Images of the initial state of the freestanding MTSI and the front and side views when stretched by 150% (from top to bottom). b) Stress–strain curves of a dog-bone-shaped copper plate (thickness t_{inter} = 100 µm) in uniaxial tension. c–k) Curves of the force versus the applied strain during the first applied stretch, unloading, and second applied stretch; the first applied strain for (c–k) is 30%, 50%, 60%, 75%, 90%, 110%, 120%, 130%, and 150%, respectively ((i–k) contain the FEA results, dotted lines).

The fatigue life of the MTSI is a crucial problem that needs to be investigated because of its yielded plasticity. For structures subjected to cyclic loading, if plastic deformation occurs only during the first few cycles and only elastic deformation occurs in the following cycles, the structure is in a shakedown state. According to the shakedown theory,[34,35] a structure in the shakedown state is safe from low-cycle fatigue damage. In this study, the overstretch strategy yields plasticity only during the first applied stretch and reverse displacement unloading, that is, the MTSI is in a shakedown state. Thus, the plasticity caused by the overstretch strategy does not significantly reduce the fatigue life of the electronics. A fatigue test of the MTSI is carried out to further investigate the effect of the overstretch strategy on fatigue life. A cyclic strain of 120% is applied to the freestanding MTSI, and its resistance is monitored. After 10 000 cycles, the MTSI is not significantly damaged, and the electrical properties are not affected (Figure S5, Supporting Information Appendix). This indicates that the fatigue life of the present MTSI subjected to an enhanced stretching strain is greater than 10 000 cycles, which is sufficient for many working conditions. In addition, we investigate the influence of the plasticity yielded by overstretch strategy on electric performance by applying a cyclic strain of 150% to the MTSI and monitoring its resistance. After four cycles, the MTSI resistance is less affected by plastic deformation (Figure S6, Supporting Information Appendix).

2.3. Mechanical Analysis of the MTSI Bonded on the Soft Substrate

In practical flexible electronics, the stretchable structures are usually bonded on soft substrates for encapsulation and protection. Figure 2 has preliminarily verified that the overstretch strategy is valid for the MTSI bonded on the soft substrate. To explore the effect of the overstretch strategy on the elastic stretchability of interconnects with different geometries, a series of finite element analyses is performed for the commonly used horseshoe, zigzag, and fractal structures, as shown in **Figure 5**a–c. The material parameters and thicknesses of the interconnect and substrate are consistent with the model shown in Figure 2, and the details of the in-plane layouts are presented in Figure S7 (Supporting Information Appendix). Figure 5a–c presents the enhanced elastic stretchability of the horseshoe/zigzag/fractal interconnects as a function of the maximum of the first applied strain. The elastic stretchability of the horseshoe/zigzag/fractal interconnects is not enhanced when the maximum of the first applied strain does not exceed the designed elastic stretchability $\epsilon_{\text{designed-elastic}}$ (7.43%/9.47%/78.6%). If the maximum of the first applied strain (overstrain) 7.43% < $\epsilon_{\text{over}} \leq$ 14.86%/9.47% < $\epsilon_{\text{over}} \leq$ 18.94%/78.6% < $\epsilon_{\text{over}} \leq$ 157.2%, no additional plasticity exists in the horseshoe/zigzag/fractal interconnects during releasing the first applied strain. The elastic stretchability of the horseshoe/zigzag/fractal interconnects is enhanced to $\epsilon_{\text{enhanced-elasti}}\text{c} = \epsilon_{\text{over}}$. When the overstrain $\epsilon_{\text{over}} >$ 14.86%/$\epsilon_{\text{over}} >$ 18.94%/$\epsilon_{\text{over}} >$ 157.2%, additional plasticity is observed in the horseshoe/zigzag/fractal interconnects when releasing the first applied strain. Similar to the freestanding MTSI, the enhanced elastic stretchability does not exceed twice the designed elastic stretchability $\epsilon_{\text{enhanced-elastic}}$ = 14.86%/$\epsilon_{\text{enhanced-elastic}}$ = 18.94%/$\epsilon_{\text{enhanced-elastic}}$ = 157.2%. The above FEA analysis demonstrates that the overstretch strategy is effective not only for the MTSI bonded on the soft substrates but also for thick interconnects with various geometrical layouts, such as horseshoe and fractal interconnects.

A previous study by the authors reveals that the thickness of the interconnects significantly affects the deformation mode and elastic stretchability,[16] as shown in Figure 5d, with serpentine interconnects as an example. As the thickness of the interconnects increases, the deformation mode changes from wrinkling/buckling to non-buckling, and the designed elastic stretchability first increases, then decreases, and increases again until it becomes stable. Three representative cases with different thicknesses and the corresponding deformation modes, shown in Figure 5d, are selected to study the effect of the overstretch strategy. For interconnects with thicknesses of 0.05 μm and 2 μm, the deformation modes are wrinkling and buckling, as shown in Figure 5e,f, respectively. The designed elastic stretchabilities of the interconnect with thicknesses 0.05 μm and 2 μm are 17.7% and 31%, respectively, and the corresponding enhanced elastic stretchabilities are 44.4% and 75.8%, respectively; these values are more than twice the corresponding designed elastic stretchabilities. In contrast to the cases with thick interconnects, the enhanced elastic stretchability of thin interconnects finally decreases gradually with an increase in overstrain. To understand the underlying mechanism, the strain contours and deformation of the structures are analyzed, as shown in Figures S8 and S9 (Supporting Information Appendix). This can be attributed to the formation of out-of-plane wrinkles or bending. Figure 5h shows a comparison of the deformation modes of the partial semicircle for thick and thin interconnects. It can be observed that only in-plane deformation occurs for the thick interconnects during the first applied strain, unloading, and second applied strain, and the enhance elastic stretchability cannot exceed twice the designed elastic stretchability. For thin interconnects, the unloading process can be purely elastic owing to the adoption of both the deformation modes of compression and out-of-plane wrinkling/bending, even though the overstrain is more than twice the designed elastic stretchability. Conversely, the enhanced elastic stretchability can be more than twice the designed elastic stretchability. However, if plasticity occurs during the unloading process for a larger overstrain, the enhanced elastic stretchability may be lower than the overstrain. Subsequently, the enhanced elastic stretchability decreases as the overstrain increases, as shown in Figure 5e,f. Figure 5g shows the deformation mode and analysis of the stretchability of the MTSI with thickness t_{inter} = 200 μm. The designed elastic stretchability is 59%, whereas the enhanced elastic stretchability is 118%. Additionally, the effect of the substrate modulus on the elastic stretchability of MTSI is investigated. Figure S10 (Supporting Information Appendix) shows that the designed/enhanced elastic stretchability of the MTSI decreases as the modulus of the substrate increases. However, the overstretch strategy can double the structure stretchability regardless of the substrate type. For extreme comparison, we conduct stretching experiments using the MTSI bonded to the Ecoflex substrate with 60 kPa and the freestanding MTSI. The deformation modes for the two cases are almost the same, with minute differences regarding the detailed deformation (Figure S11, Supporting Information Appendix). These also

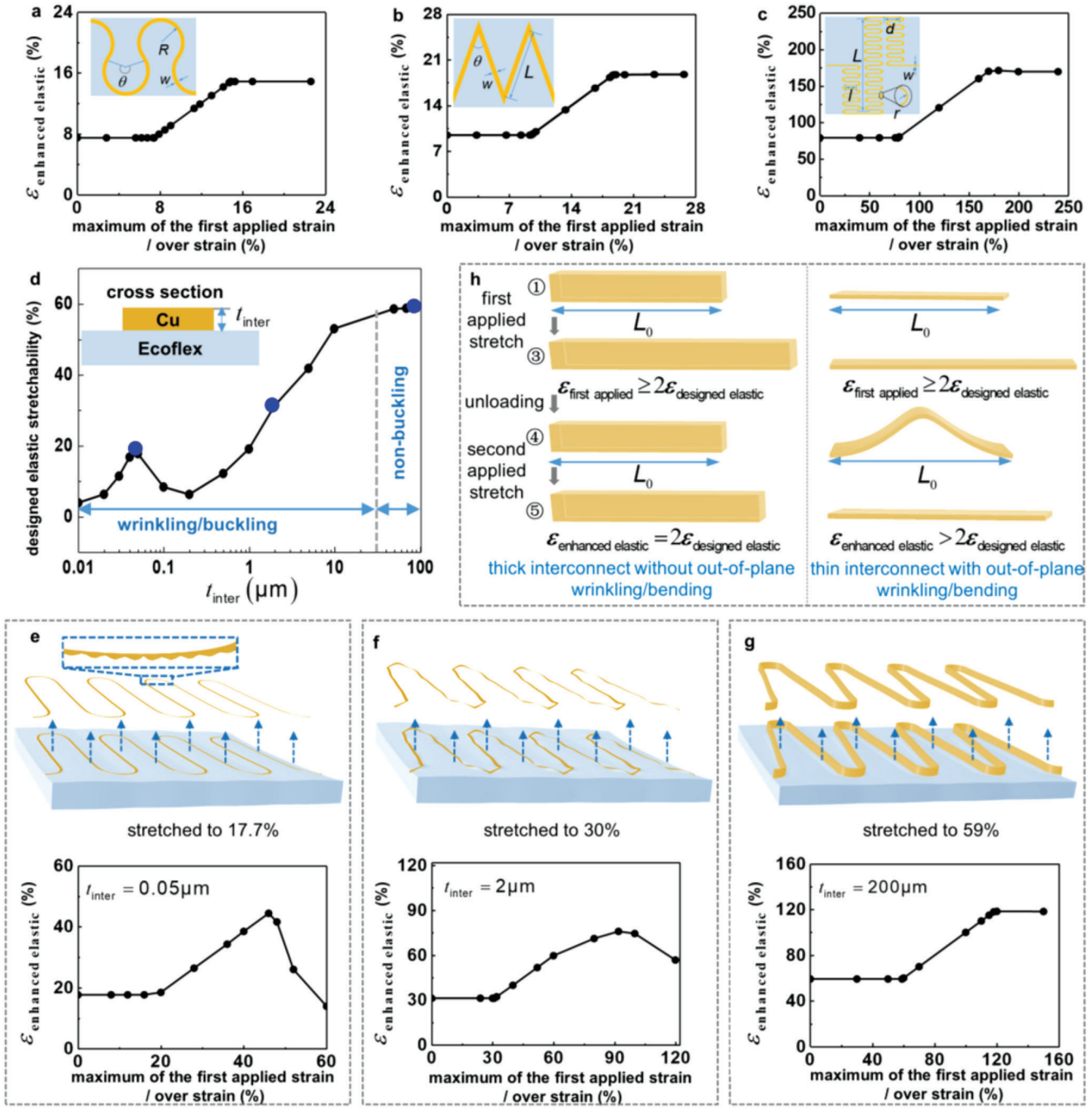

Figure 5. Mechanical analysis of the MTSI bonded on the soft substrate. a–c) The enhanced elastic stretchability of thick horseshoe/zigzag/fractal interconnects bonded on the soft substrate as a function of the maximum of the first applied strain/overstrain. d) Curve of the designed elastic stretchability of serpentine interconnection bonded on the soft substrate as a function of its thickness. e–g) FEA results of serpentine interconnections with three typical thicknesses (0.05 μm, 2 μm,200 μm). The upper subgraphs are the corresponding wrinkling, buckling, and non-buckling deformation during stretching, and the lower subgraphs show the relationship between the enhanced elastic stretchability of the structure and the maximum of the first applied strain/overstrain. h) Schematic of the deformation modes of the partial semicircle for the thick and thin interconnects.

suggest that it is reasonable to verify the effectiveness of overstretch strategy by the freestanding MTSI.

The novelty of this study is that a new strategy to enhance elastic stretchability, completely different from the existing strategies of using a prestrained elastic substrate and designing geometric layouts, is proposed. The overstretch strategy is clearly different from the geometric design strategy and can be combined with the geometric design strategy to enhance elastic stretchability. Comparing the prestrain and overstretch strategies shows that the overstretch is applied after the transfer-printing operation, whereas the prestrain is applied before the transfer-printing operation (Figure S12, Supporting Information Appendix). From this

perspective, the overstretch strategy allows easier fabrication and is more conducive to mass production. The overstretch strategy of stretchable electronics is first proposed in this study; therefore, several aspects related to the overstretch strategy are yet to be investigated. These aspects include the mechanical analysis of theoretical and experimental results of interconnects bonded to a soft substrate. This is an interesting and challenging problem, and further studies will be conducted to investigate other methods in the future.

3. Conclusion

This study proposes an overstretch strategy to enhance the elastic stretchability beyond the designed elastic range of stretchable structures by applying an overstretch after transfer printing and bonding to a soft substrate. Using a typical freestanding MTSI as an example, the theoretical, numerical, and experimental results collectively reveal that the overstretch strategy can double the designed elastic stretchability; this is crucial to realize the good performance of stretchable electronics. The underlying mechanism considers the evolution of the elastoplastic constitutive relation during overstretching to double the elastic range of the critical part of the stretchable structure. Further numerical analysis validates the overstretch strategy for various geometrical interconnects bonded to soft substrates, including horseshoe, zigzag, and fractal interconnects, with both thick and thin cross-sections. In particular, the stretchability of interconnects with thin cross-sections can be enhanced to more than twice the designed elastic stretchability. Compared to the existing strategies of using the prestrained elastic substrate and designing geometric layouts, the proposed overstretch strategy is easier to operate in practice. Furthermore, these three strategies can be selectively combined to enhance the elastic stretchability of stretchable electronics. As the proposed overstretch strategy provides a new route for enhancing elastic stretchability, it may significantly promote the development and application of stretchable electronics in the future.

4. Experimental Section

Preparation of the MTSI: The MTSI was fabricated by cutting 100-µm-thick copper plates (99.99%) using a P-second laser precision machining system (DCT-DL566PU, China, as shown in Figure S13, Supporting Information Appendix). The laser power was adjusted to 75% of the maximum power, and laser cutting was performed for 300 cycles.

Mechanical Testing of the MTSI: Tensile testing of the MTSIs was performed with an ElectroForce system (3100 series, USA, the precision of 0.1 mN, Figure S14, Supporting Information Appendix). A displacement-control loading mode was adopted. To demonstrate all cases of the overstretch strategy, the maximum values of the first applied strain/overstrain were chosen as 30%, 50%, 60%, 75%, 90%, 110%, 120%, 130%, and 150%. After reverse displacement was unloaded to zero applied strain, the second applied strain reached 200%.

Mechanical Testing of the Constitutive Model of the Copper Plates: The specimens (Figure S15, Supporting Information Appendix) were fabricated by cutting 100-µm-thick copper plates (99.99%) using a P-second laser precision machining system (Figure S13, Supporting Information Appendix). Tensile testing of the copper plate was performed using an electronic material-testing machine (Instron 5942, USA, Figure S16, Supporting Information Appendix).

Finite Element Analyses: The FEA was performed using the commercial software package ABAQUS (SIMULIA, France). A half-period of the MTSI was used for the FEA model, with the boundary conditions of a displacement load in the x-direction. The elements of C3D8 and C3D8R were used as the soft substrates and metal interconnects, respectively.

Supporting Information

Supporting Information is available from the Wiley Online Library or from the author.

Acknowledgements

Y.S. gratefully acknowledges support from the National Natural Science Foundation of China (Grant No. 12172359 and 11772331), Beijing Municipal Natural Science Foundation (No. 2202066), Key Research Program of Frontier Sciences of the Chinese Academy of Sciences (ZDBS-LY-JSC014), and CAS Interdisciplinary Innovation Team (JCTD-2020-03).

Conflict of Interest

The authors declare no conflict of interest.

Author Contributions

Y.S. conceived the study. J.L. and Y.S. conducted the theoretical derivation, experimental fabrication, and performance tests. J.L., X.W., and Y.S. discussed all the data and prepared the manuscript. Y.S. supervised the study.

Data Availability Statement

Research data are not shared.

Keywords

elastic stretchabilities, overstretch strategies, serpentine interconnects, stretchable electronics

Received: January 11, 2023
Revised: March 29, 2023
Published online: May 24, 2023

[1] G. Schwartz, B. C. K. Tee, J. Mei, A. L. Appleton, D. H. Kim, H. Wang, Z. Bao, *Nat. Commun.* **2013**, *4*, 1859.
[2] H. Liu, H. Zhao, S. Li, J. Hu, X. Zheng, R. Li, Y. Chen, Y. Su, *Adv. Mater. Technol.* **2019**, *4*, 1800327.
[3] H. Jeong, J. Y. Lee, K. H. Lee, Y. J. Kang, J. T. Kim, R. Avila, A. Tzavelis, J. Kim, H. Ryu, S. S. Kwak, J. U. Kim, A. Banks, H. Jang, J. K. Chang, S. Li, C. K. Mummidisetty, Y. Park, S. Nappi, K. S. Chun, Y. J. Lee, K. Kwon, X. Ni, H. U. Chung, H. Luan, J. H. Kim, C. Wu, S. Xu, A. Banks, A. Jayaraman, Y. Huang, et al., *Sci. Adv.* **2021**, *7*, 20.
[4] D. Lu, Y. Yan, R. Avila, I. Kandela, I. Stepien, M. H. Seo, W. Bai, Q. Yang, C. Li, C. R. Haney, E. A. Waters, M. R. MacEwan, Y. Huang, W. Z. Ray, J. A. Rogers, *Adv. Healthcare Mater.* **2020**, *9*, e2000942.
[5] S. R. Krishnan, C.-J. Su, Z. Xie, M. Patel, S. R. Madhvapathy, Y. Xu, J. Freudman, B. Ng, S. Y. Heo, H. Wang, T. R. Ray, J. Leshock, I. Stankiewicz, X. Feng, Y. Huang, P. Gutruf, J. A. Rogers, *Small* **2018**, *14*, 1870226.

[6] F. Zhang, Y. Zang, D. Huang, C. A. Di, D. Zhu, *Nat. Commun.* **2015**, *6*, 8356.
[7] L. Zhang, X. Jiang, W. Jiang, S. Li, Y. Chi, H. Liu, M. Zhang, J. Li, M. Fang, B. Pan, Y. Chen, C. Shen, X. Guo, R. Li, L. Guo, Y. Su, *Adv. Mater. Technol.* **2019**, *4*, 1900150.
[8] A. D. Mickle, S. M. Won, K. N. Noh, J. Yoon, K. W. Meacham, Y. Xue, L. A. McIlvried, B. A. Copits, V. K. Samineni, K. E. Crawford, D. H. Kim, P. Srivastava, B. H. Kim, S. Min, Y. Shiuan, Y. Yun, M. A. Payne, J. Zhang, H. Jang, Y. Li, H. H. Lai, Y. Huang, S. Il Park, R. W. Gereau, J. A. Rogers, *Nature* **2019**, *565*, 361.
[9] X. Yu, H. Wang, X. Ning, R. Sun, H. Albadawi, M. Salomao, A. C. Silva, Y. Yu, L. Tian, A. Koh, C. M. Lee, A. Chempakasseril, P. Tian, M. Pharr, J. Yuan, Y. Huang, R. Oklu, J. A. Rogers, *Nat. Biomed. Eng.* **2018**, *2*, 165.
[10] D. Floreano, R. Pericet-Camara, S. Viollet, F. Ruffier, A. Brückner, R. Leitel, W. Buss, M. Menouni, F. Expert, R. Juston, M. K. Dobrzynski, G. L'Eplattenier, F. Recktenwald, H. A. Mallot, N. Franceschini, *Proc. Natl. Acad. Sci. U. S. A.* **2013**, *110*, 9267.
[11] H. Hu, X. Zhu, C. Wang, L. Zhang, X. Li, S. Lee, Z. Huang, R. Chen, Z. Chen, C. Wang, Y. Gu, Y. Chen, Y. Lei, T. Zhang, N. Kim, Y. Guo, Y. Teng, W. Zhou, Y. Li, A. Nomoto, S. Sternini, Q. Zhou, M. Pharr, F. L. d. Scalea, S. Xu, *Sci. Adv.* **2018**, *4*, 2069.
[12] C. Cochrane, M. Lewandowski, A. V. Koncar, *Sensors* **2010**, *10*, 8291.
[13] Y. Zhang, S. Wang, X. Li, J. A. Fan, S. Xu, Y. M. Song, K. J. Choi, W. H. Yeo, W. Lee, S. N. Nazaar, B. Lu, L. Yin, K. C. Hwang, J. A. Rogers, Y. Huang, *Adv. Funct. Mater.* **2014**, *24*, 2028.
[14] R. Pelrine, R. Kornbluh, J. Joseph, R. Heydt, Q. Pei, S. Chiba, *Mater. Sci. Eng., C* **2000**, *11*, 89.
[15] H. C. Ko, M. P. Stoykovich, J. Song, V. Malyarchuk, W. M. Choi, C. J. Yu, J. B. Geddes, J. Xiao, S. Wang, Y. Huang, J. A. Rogers, *Nature* **2008**, *454*, 748.
[16] Y. Su, X. Ping, K. J. Yu, J. W. Lee, J. A. Fan, B. Wang, M. Li, R. Li, D. v. Harburg, Y. A. Huang, C. Yu, S. Mao, J. Shim, Q. Yang, P. Y. Lee, A. Armonas, K. J. Choi, Y. Yang, U. Paik, T. Chang, T. J. Dawidczyk, Y. Huang, S. Wang, J. A. Rogers, *Adv. Mater.* **2017**, *29*, 1604989.
[17] M. Gonzalez, F. Axisa, M. Vanden Bulcke, D. Brosteaux, B. Vandevelde, J. Vanfleteren, *Microelectron. Reliab.* **2008**, *48*, 825.
[18] D. S. Gray, J. Tien, C. S. Chen, *Adv. Mater.* **2004**, *16*, 393.
[19] D.-Y. Khang, H. Jiang, Y. Huang, J. A. Rogers, *Science* **2006**, *311*, 208.
[20] D. H. Kim, J. Song, M. C. Won, H. S. Kim, R. H. Kim, Z. Liu, Y. Y. Huang, K. C. Hwang, Y. W. Zhang, J. A. Rogers, *Proc. Natl. Acad. Sci. U. S. A.* **2008**, *105*, 18675.
[21] S. Xu, Y. Zhang, J. Cho, J. Lee, X. Huang, L. Jia, J. A. Fan, Y. Su, J. Su, H. Zhang, H. Cheng, B. Lu, C. Yu, C. Chuang, T. Il Kim, T. Song, K. Shigeta, S. Kang, C. Dagdeviren, I. Petrov, P. V. Braun, Y. Huang, U. Paik, J. A. Rogers, *Nat. Commun.* **2013**, *4*, 1543.
[22] Z. Xue, T. Jin, S. Xu, K. Bai, Q. He, F. Zhang, X. Cheng, Z. Ji, W. Pang, Z. Shen, H. Song, Y. Shuai, Y. Zhang, *Sci. Adv.* **2022**, *8*, 6922.
[23] H. Zhao, X. Cheng, C. Wu, T. L. Liu, Q. Zhao, S. Li, X. Ni, S. Yao, M. Han, Y. Huang, Y. Zhang, J. A. Rogers, *Adv. Mater.* **2022**, *34*, 2109416.
[24] M. Li, J. Xia, R. Li, Z. Kang, Y. Su, *J. Mater. Sci.* **2013**, *48*, 8443.
[25] D. H. Kim, N. Lu, R. Ma, Y. S. Kim, R. H. Kim, S. Wang, J. Wu, S. M. Won, H. Tao, A. Islam, K. J. Yu, T. Il Kim, R. Chowdhury, M. Ying, L. Xu, M. Li, H. J. Chung, H. Keum, M. McCormick, P. Liu, Y. W. Zhang, F. G. Omenetto, Y. Huang, T. Coleman, J. A. Rogers, *Science* **2011**, *333*, 838.
[26] C. Yu, Z. Duan, P. Yuan, Y. Li, Y. Su, X. Zhang, Y. Pan, L. L. Dai, R. G. Nuzzo, Y. Huang, H. Jiang, J. A. Rogers, *Adv. Mater.* **2013**, *25*, 1541.
[27] Y. Zhang, H. Fu, Y. Su, S. Xu, H. Cheng, J. A. Fan, K. C. Hwang, J. A. Rogers, Y. Huang, *Acta. Mater.* **2013**, *61*, 7816.
[28] J. A. Fan, W. H. Yeo, Y. Su, Y. Hattori, W. Lee, S. Y. Jung, Y. Zhang, Z. Liu, H. Cheng, L. Falgout, M. Bajema, T. Coleman, D. Gregoire, R. J. Larsen, Y. Huang, J. A. Rogers, *Nat. Commun.* **2014**, *5*, 3266.
[29] Y. Zhang, H. Fu, S. Xu, J. A. Fan, K. C. Hwang, J. Jiang, J. A. Rogers, Y. Huang, *J. Mech. Phys. Solids* **2014**, *72*, 115.
[30] Y. Su, S. Wang, Y. A. Huang, H. Luan, W. Dong, J. A. Fan, Q. Yang, J. A. Rogers, Y. Huang, *Small* **2015**, *11*, 367.
[31] H. Liu, R. Y. Xue, J. Q. Hu, X. C. Ping, H. P. Wu, M. Q. Huang, H. Zhang, X. Guo, R. Li, Y. L. Chen, Y. W. Su, *Sci. China: Phys., Mech. Astron.* **2018**, *61*, 114611.
[32] Y. Yu, J. Guo, L. Sun, X. Zhang, Y. Zhao, *Research* **2019**, *2019*, 6906275.
[33] X. Guo, X. Ni, J. Li, H. Zhang, F. Zhang, H. Yu, J. Wu, Y. Bai, H. Lei, Y. Huang, J. A. Rogers, Y. Zhang, *Adv. Mater.* **2021**, *33*, 2004919.
[34] C. Polizzotto, *J. Appl. Mech.* **1993**, *6*, 20.
[35] H.-S. Yu, *Plasticity and Geotechnics*, Springer, New York, **2006**.